Design of a Vibrotactile Display via a Rigid Surface

Yon Visell and Jeremy R. Cooperstock
McGill University, Montreal, Canada

ABSTRACT

This paper describes the analysis, optimized redesign and evaluation of a high fidelity vibrotactile display system integrated in a rigid surface. The main application of the embodiment described here is vibrotactile display of virtual ground surface material properties for immersive environments, although the design principles are general. The device consists of a light, composite plate mounted on an elastic suspension with integrated force sensors. It is actuated by a single voice coil motor. The structural dynamics of the device were optimized within the constraints imposed by the requirements of user interaction. They were further corrected via digitally implemented inverse filtering. Measurements of the resulting display demonstrate that it is capable of accurately reproducing forces of more than 40 N across a usable frequency band from 50 Hz to 750 Hz.

1 INTRODUCTION

Vibrotactile display devices consist of palpable interfaces that are capable of vibrating at frequencies salient to human tactile perception, but are not necessarily capable of static force display. Advantages of such displays include their low cost, power efficiency, and capability of rendering transient or textural effects accurately, at high temporal resolution, when suitable actuators are used.

Here, we report on the design of a vibrotactile display device integrated in a rigid, quasi-static plate. The specific embodiment this work has addressed is tailored to vibrotactile interaction between feet and instrumented floor surfaces. Potential applications of such a device include the rendering of virtual ground textures for virtual and augmented reality simulation [16] or telepresence (e.g., for remote planetary simulation), the rendering of specific ground effects or other ecological cues for rehabilitation, or the provision of tactile feedback for virtual foot controls, control surfaces, or other interfaces. The device presented here constitutes an extensive redesign and optimization of a similar interface that was introduced in earlier work by the authors [13]. Here, our intention is to systematically specify the device in such a way as to ensure a transparent display fidelity, suitable for use in perceptual experiments. We also aim to provide sufficient documentation that it may reproduced by other researchers or practitioners interested in vibrotactile display via floor surfaces, or related issues in perception and interaction design. The sections that follow present the mechanical and electronic structure of the new device, the analysis and optimization that were undertaken to improve its dynamic response, and point to future directions in this line of research.

2 COMPONENTS

2.1 Mechanical Structure

The mechanical design is broadly similar to that of the original device, but accounts better for both the static and dynamic performance requirements for the display. The top plate provides an interface to the body, which in the case of our device is assumed to consist of a foot wearing a shoe. Statically, the device must resist bending when loaded vertically by a force of several hundred Newtons. The rigid deflection of the plate under this load must be minimized subject to the constraint that the plate be able to vibrate freely. This trade-off is analyzed in Section 3.3.

The top plate consists of a commercially manufactured aluminum honeycomb sandwich panel component (MSC model 0513 SSP) with dimensions $30.4 \times 30.4 \times 2.54$ cm and a weight of 400 g. The panel has aluminum facings with a thickness of 0.08 cm. This material was selected for its high bending stiffness to weight ratio. The panel sides are closed with a basswood veneer to eliminate acoustic emissions that otherwise result from small deflections of the honeycomb at the edges of the panel. The plate is supported by cylindrical SBR rubber elastic elements positioned as shown in Fig. 1. In dynamic or multi-tile configurations, a retaining socket surrounding the elastic support (not present in the figure) is used to keep the plate from changing position. The actuator is mounted via an aluminum bracket bonded to the center underside of the plate.

2.2 Sensing

In order to render an interactive response from a virtual ground surface using the kinds of models we have developed (Sec. 5), it is necessary to capture the normal force applied to the tile by the user's foot. Positioning the force sensors beneath the plate is feasible, since the bandwidth of the force applied to the plate by the user is limited. In the design presented here, the sensors are furthermore positioned beneath the elastic suspension of the device, so as to better isolate them from the actuators.

Force sensing is performed via four load cell force transducers (Measurement Systems model FX19) located below the vibration mount located under each corner of the plate. Although the cost for outfitting a single-plate device with these sensors is not prohibitive, many of the applications we have in mind consist of two dimensional $m \times n$ arrays of tiles, requiring a number $N = 4mn$ of sensors. As a result, in a second configuration, four low-cost resistive force sensors (Interlink model 402 FSR) are used in place of load cells. After conditioning, the response of these sensors to an applied force is nonlinear, and varies up to 25% from part to part (according to manufacturer ratings). Consequently, a measurement and subsequent linearization and force calibration of each is performed, using a calibrated load cell force sensor (details are provided in a companion publication [16]). After such a calibration, a linear response accurate to within $\pm 2.5\%$ can be obtained using low cost parts.

2.3 Actuation

The tile is actuated by a single Lorentz force type voice coil motor (Clark Synthesis model TST429) with a nominal impedance of 6 Ohms. The actuator is coupled to the tile by a 1.25 cm diameter threaded rod interfacing with an aluminum bracket, as shown in Fig. 1. The actuator has a usable bandwidth of about 25 Hz to 20 kHz, and is capable of driving the plate above strongly enough to quickly produce numbness in the region of the foot that is in contact with the tile.

2.4 Electronics

Analog data from the force sensors is conditioned, amplified, and digitized via a custom acquisition board, based on an Altera FPGA,

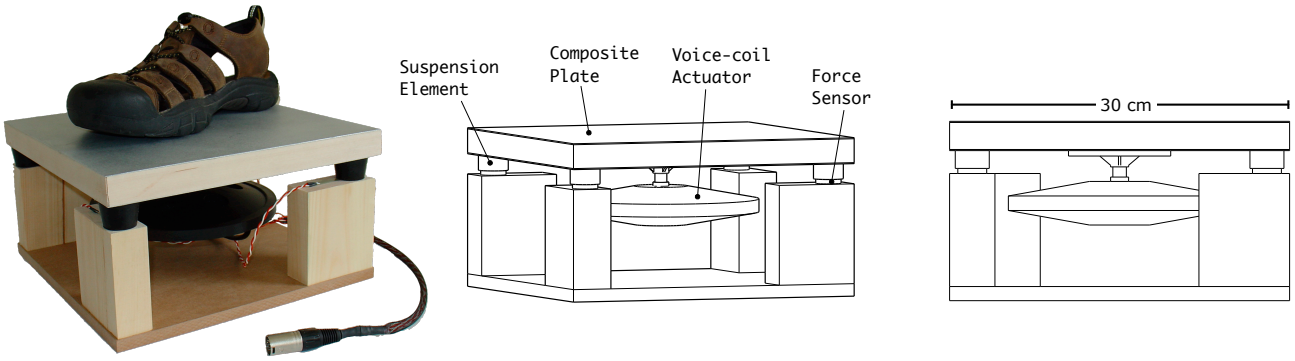

Figure 1: Vibrotactile floor interface hardware for a single tile unit. Left: Photo with large mens' shoe, showing representative size. The model shown is based on the low-cost force sensing resistor option. The cable in the foreground interfaces with the sensors. Middle: View showing main components. Right: Side view with top dimension.

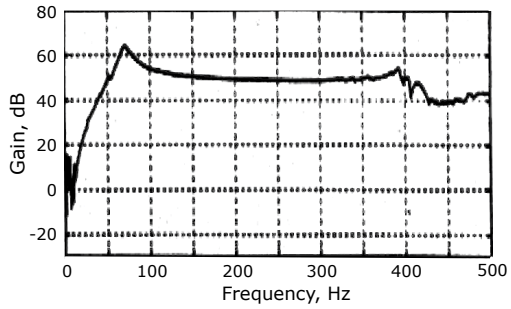

Figure 2: Typical actuator frequency response (manufacturer supplied data, permission pending).

with 16-bit analog-to-digital converters. Data from each sensor is sampled at a rate of 1 kHz and transported to a host computer over UDP via the board's 10 Mbps Ethernet interface. Digital to analog conversion of the signal driving the actuator is performed using a low noise 24-bit, 96 kHz audio interface (Edirol model FA-101), and amplification is performed using a compact, class-D audio amplifier based on the Tripath TK2050. The amplifier is rated as capable of providing 100 W to a nominal 4 Ohm actuator impedance.

3 Dynamic Response

The main factors affecting the dynamic response of the device are the actuator characteristics, the dynamics of the rigid plate, and that of the elastic suspension. In a suitable regime, one may regard these as lumped linear systems, with respective Laplace transform domain transfer functions $H_a(s), H_p(s)$ and $H_s(s)$. The corresponding model device transfer function can be given by $H_d(s) = H_a(s)H_p(s)H_s(s)$. However, the spatial configuration of these elements relative to each other also contributes to the structural dynamics of the display.

3.1 Actuator Response

Fig. 2 shows a typical amplitude frequency response for this family of actuators, based on data supplied by the manufacturer. The data was acquired from an accelerometer attached to the mounting bold, with the actuator attached to a rigid wooden surface. The shape of this nominal response affects that of our device (Sec. 4).

3.2 Plate Response

The contribution of the interface plate to the dynamic response of the device can be predicted in terms of the vibrational characteristics of the plate, and the coupling between plate and actuator.

3.2.1 Free response

In the case of a homogeneous, isotropic plate, the free vibrations of interest are governed by a partial differential equation of motion for bending wave displacements. In the thin plate approximation, it is [3]:

$$\rho h \frac{\partial^2 z}{\partial t^2} + D\nabla^4 z = 0, \quad D = \frac{Eh^3}{12(1-\nu^2)} \tag{1}$$

Here, $z = z(\mathbf{r},t)$ is displacement, $\mathbf{r} = (x,y)$ is a position on the tile surface, t is time, E and ν are the Young's modulus and Poisson's ratio of the plate material, ρ is its mass density, and h is the plate thickness, D is known as the flexural stiffness, and we neglect effects of damping.

Below the first resonant frequency of the plate, f_1, the vibrational response is well approximated by that of an ideal, rigid mass coupled to an elastic suspension (Sec. 3.3 below). Since we seek a usable display bandwidth with upper limit of 1 kHz, we want to ensure that $f_1 > 1$ kHz. For a rectangular, homogeneous, isotropic plate, the frequencies of the normal modes of bending oscillation are of the form [3]:

$$f(k) = \frac{hk^2}{2\pi}\sqrt{\frac{D}{\rho h}}, \quad k \propto L^{-1} \tag{2}$$

Here, k is the magnitude of the wavenumber vector $\mathbf{k} = (k_x, k_y)$ of the oscillation, and L^{-1} is the inverse length of the plate, and x and y are the directions tangent to the plate surface parallel to its edges. For pure simply supported boundary conditions (which are never achieved in practice), $k_x = m\pi/L$ and $k_y = n\pi/L$, where m and n are positive (non-zero) integers [3]. The lowest frequency mode is $f_1 = f(|\mathbf{k}_1|)$, with $\mathbf{k}_1 = (\pi/L, \pi/L)$. The amplitudes of the normal modes are

$$\eta_{mn}(\mathbf{r}) = \sin(k_x x)\sin(k_y y) \tag{3}$$

The value of the Poisson's ratio-dependent factor $(1-\nu^2)^{-1/2}$ in Eq. 1 lies in a range from 1.0 to 1.16 for solid materials such as are considered here, so in a first approximation we may ignore it. In order to maximize the frequency $f(k)$ for any given value of the wavenumber magnitude k and given plate geometric properties L and h, the plate material should be selected to possess a high

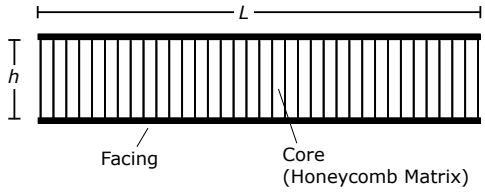

Figure 3: A composite sandwich plate, shown in profile (side view). It consists of a stiff, solid facing material bonded (typically laminated) to a lightweight core, such as a metal or kevlar honeycomb matrix.

stiffness E and low mass density ρ. While solid, isotropic materials such as metals can achieve a high stiffness, their mass density is typically commensurately higher, which is a limitation. In addition, their mass grows linearly with thickness, making them less efficient to actuate. In practice, for a solid plywood plate (light enough to be efficiently actuated) with dimensions 30.4 cm $\times$ 30.4 cm $\times$ 3.75 cm, one finds $f_1 \approx 400$ Hz, which falls short of the design target.

3.2.2 Composite plate

A class of structures that achieves higher stiffness-to-mass ratios than is possible with uniform solids is that of composite sandwiches. Such a panel is formed via the use of thin layers of stiff solid material bonded to a lightweight core. Fig. 3 illustrates a composite sandwich of the type used in our device. The core consists of an aluminum honeycomb matrix, while the facing materials consist of aluminum sheet. The bending stiffness of such a material is approximately given by $E \approx \sqrt{3} E_f t_f / h$ [4], where E_f is the Young's modulus of the facing material, t_f is the thickness of the facing material, and h is the core thickness (Fig. 3). To a first approximation, the frequencies of the normal modes of bending oscillation of such a composite sandwich plate can be obtained[1] substituting this expression for E into Eq. 2. The resulting frequencies are:

$$f(k) = \frac{k^2}{2\pi} \sqrt{\frac{E_f t_f h}{12\rho}}, \quad k \propto L^{-1} \tag{4}$$

Again, the admissible values of k depend on the boundary conditions. This equation (which is valid only for thin facings $t_f \ll h$) depends on the stiffness E_f of the facing material and the average mass density of the entire panel. For our device, assuming idealized boundary conditions, the minimum value of k is $\pi\sqrt{2}/L$ (see Sec. 3.4). The other factors are given by: $h = 2.5$ cm, $t_f = 0.083$ cm, $E_f \approx 60$ GPa, and $\rho \approx 170$ kg / m^3. For these values, Eq. (4) yields $f_1 \approx 845$ Hz. This overestimates the measured value of f_1 for our device by approximately 10% (Sec. 4).

3.2.3 Actuator coupling

The actuated plate is driven by a surface force distribution $F(\mathbf{r},t)$, and the resulting equation of motion possesses a driving term:

$$\rho h \frac{\partial^2 z}{\partial t^2} + D\nabla^4 z = F(\mathbf{r},t) \tag{5}$$

For our device, the latter can be modeled as $F(\mathbf{r},t) = F(t)\phi(\mathbf{r})$, where $F(t)$ is the actuator force amplitude, and $\phi(\mathbf{r})$ approximates a spatial Dirac delta function $\delta(\mathbf{r}-\mathbf{r}_0)$ centered at the tile midpoint. Generalizing slightly, one can consider the case of N independent point actuators at locations $\mathbf{r}_i$, in which case $F(\mathbf{r}) = \sum_{i=1}^{N} F_i(t)\delta(\mathbf{r}-\mathbf{r}_i)$, where F_i is the force signal from the ith actuator.

[1] The authors did not find this expression for $f(k)$ in the research literature, but approximations like it are presumably well-known.

An arbitrary displacement $z(\mathbf{r},t)$ can be expanded in the normal modes $\eta_{mn}(\mathbf{r})$ of vibration, yielding modal coordinates $Z_{mn}(t)$ defined by:

$$z(\mathbf{r},t) = \sum_{m,n\geq 0} Z_{mn}(t)\eta_{mn}(\mathbf{r}), \text{ where} \tag{6}$$

$$Z_{mn}(t) = \int z(\mathbf{r},t)\eta_{mn}(\mathbf{r}) d^2\mathbf{r} \tag{7}$$

In these coordinates, the equation of motion is [6]:

$$\left(\frac{\partial^2}{\partial t^2} + \omega_{mn}^2\right) Z_{mn}(t) = \sum_i \eta_{mn}(\mathbf{r}_i) F_i(t) \tag{8}$$

where ω_{mn} is the angular frequency of mode (m,n). Modes having nodes at the actuator location, $\eta_{mn}(\mathbf{r}_i) = 0$, satisfy the homogeneous form of Eq. (8), so are not excited by the corresponding actuator signal, and instead contribute antiresonances to the device response. As shown in Sec. 4, the bandwidth of our device is essentially limited by the antiresonance near 775 Hz for $(m,n) = (1,1)$.

3.3 Elastic Suspension

The actuator is designed to supply a force only along the direction in which it is attached, so we are primarily interested in normal modes of oscillation in the z-direction. To a first approximation, the elastic (SBR rubber) suspension may be treated as a linear, lumped element with stiffness K in the z-direction, coupled to a rigid plate with total mass M (Fig. 4). For small displacements, this stiffness is given by $K = EA/h$, where E is the Young's modulus of the suspension element, A is its vertical surface area, and h is its height. When the plate is not subjected to load from a foot, the mass $M = M_0$ is due to the plate and actuator. For the device described here, $M_0 = 2.7$ kg.

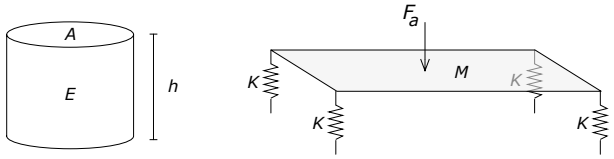

Figure 4: Left: Geometry of one elastic suspension element with height h, cross-sectional area A, and elastic modulus E. Right: Lumped model of the tile-suspension system. F_a is the actuator supplied force, $K = EA/h$ is the stiffness of a suspension element, and M is the combined mass of the actuator and tile.

Due to the symmetric placement of the actuator, there is a single dominant normal mode of oscillation, in which all suspension elements are driven in-phase in the vertical direction. The resonant frequency of this mode in the unloaded condition is given by $f_0 = (2\pi)^{-1}\sqrt{4K/M_0} = (2\pi)^{-1}\sqrt{4EA/(hM_0)}$. Above this frequency, the gain of the transfer function factor due to the suspension, $H_{susp}(f)$, is expected to be approximately constant.

A softer suspension leads to a larger response bandwidth (i.e., one with a lower frequency extent) but also to a higher static deflection δz under a load F from a foot. The latter two are related by $\delta z = F/K = Fh/(EA)$. As nominal design specifications, we aimed to select E, A and h so that $f_0 \leq 50$ Hz, so that the passband would overlap most of the frequency range of sensitivity of the FA II (Pacinian) tactile mechanoreceptors in the foot (which closely resembles the range for those in the hand [5, 12]). In addition, we aimed to achieve a deflection $\delta z \leq 5$ mm when the static force F on a single suspension element is equal to that of a large human standing at one corner (we take $F = 1000$ N). Both f_0 and δz depend only on the ratio A/h. For convenience, we choose the cross sectional area A of the suspension element to match that of the force

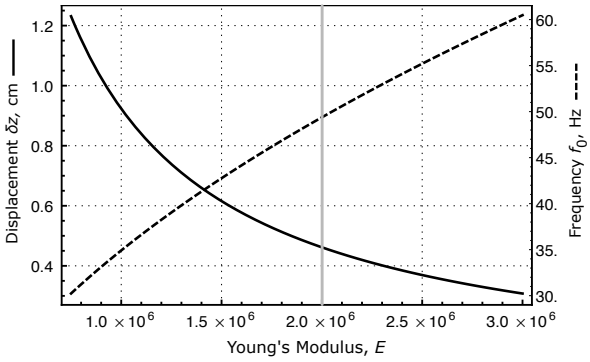

Figure 5: Resonant supension frequency f_0 and static deflection δz vs. Young's modulus for the system model with $A = 8$ cm^2 and $h = 2.5$ cm. The value $E = 2$ MPa (grey vertical line) satisfies $f_0 < 50$ Hz and $\delta z < 5$ mm.

sensor. To choose the remaining parameters, we perform a simultaneous grid search on h and E to minimize f_0 and δz. Figure 5 illustrates the dependence of f_0 and δz on E for a representative set of selected parameter values, i.e., $A = 8$ cm^2 and $h = 2.5$ cm. We selected SBR rubber vibration mounts with geometry and Young's modulus $E = 2.0$ MPa consistent with this optimization. As shown in the figure, the resulting system is expected to achieve $f_0 \approx 49$ Hz and $\delta z \approx 4.5$ mm.

3.4 Simulation

The vibrational characteristics of the tile-actuator system were simulated using finite element method (FEM) analysis. A three-dimensional geometric model of the device was designed, incorporating the sandwich panel, actuator (modeled as a homogeneous cylindrical mass), actuator bracket and connecting rod, elastic elements, and supporting structure. Material properties were assigned approximating those of the device itself, with the core honeycomb matrix replaced by a homogeneous solid with an equivalent density. Although this model entails a number of approximations, the qualitative results were expected to be correct.

3.4.1 Eigenfrequency analysis

At high frequencies, the resonant modes of the plate itself are observed. The first two are shown in Fig. 6. The lowest frequency mode has wavenumber $\mathbf{k} = (1,1)$, while the next highest resonance shown appears to correspond to a plate-induced mixture of the $(0,2)$ and $(2,0)$ modes. Their frequencies, 896 Hz and 1032 Hz, lie at a ratio of about 1.15:1.

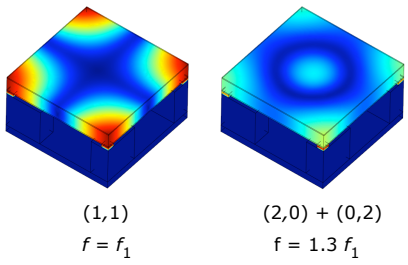

Figure 6: Visualization of the first two resonant modes of the device due to the bending mode vibrations of the plate as identified in the FEM analysis. The ring mode (right side) arises from the mixing of the plate modes indexed by the integers shown [3]. The frequencies are 896 Hz and 1032 Hz.

At low frequencies, a series of six resonances at frequencies of 28, 45, 51, and 77 Hz is observed, corresponding to deformations of the elastic support elements, in agreement with the lumped model of Sec. 3.3. The number of resonances exactly matches the six degrees of freedom of perturbation of the rigid tile. The deformation shapes recovered from the FEM analysis show that the 45 Hz resonance corresponds to oscillation in the direction normal to the plate surface; it is expected to dominate when the display is driven by the actuator.

3.4.2 Frequency response simulation

The FEM simulation of the frequency response was performed with a sinusoidal driving signal originating at the actuator. The z-axis acceleration was measured at several points on the surface of the plate, with the results shown in Fig. 7. As determined above, the cross-shaped mode gives rise to an antiresonance, due to the actuator location. The magnitude effect of these resonances, and to a secondary degree their frequency, depends substantially on the measuring point.

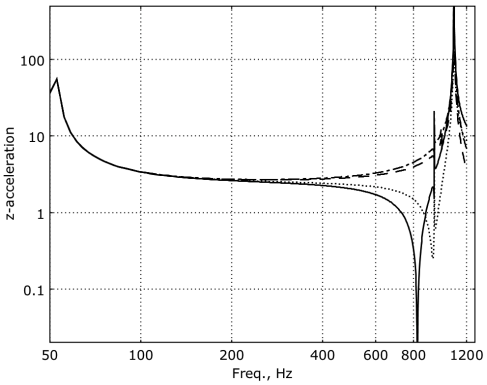

Figure 7: Results of a FEM analysis of the (acceleration) response of the device as measured at four different points on the plate surface. At frequencies below the first resonant mode, the device response is approximately constant over the surface of the plate.

4 Evaluation

Our assessment of the transparency of this device is based in part on the flatness of its magnitude frequency response over the range of perceptually salient frequencies. It is possible that achieving a linear phase response is also perceptually important. However less is known about vibrotactile sensitivity to temporal phase distortion, and to our knowledge this criterion has never been applied to the evaluation of vibrotactile displays.

4.1 Frequency response measurement

The magnitude frequency response of the device was measured by driving the plate with the actuator using the chirp method, with a slow sinusoidal frequency sweep (rate of 100 Hz / s). Measurement was performed using a piezoelectric accelerometer (AKG model CP-411) bonded to the top surface of the plate, as described in the caption of Fig. 8. Frequency response measurements were for several different foot-plate contact conditions, while the foot was wearing a rubber soled shoe. These contact conditions modify the impedance of the display, altering its response. The results are shown in Fig. 8.

The variation in the magnitude frequency response below 80 Hz is, following the analysis above, likely to be attributed to a combination of the resonant modes of the vibration suspension and the actuator response (Fig. 2). The antiresonance around 775 Hz and the resonance near 1100 Hz are due to the two lowest frequency

normal modes of the plate (Fig. 6) identified above. Variation in the range from 70 Hz to 700 Hz can be attributed in part to the actuator response. The latter (Fig. 2) includes a resonance near 70 Hz and additional coloration above 380 Hz, likely accounting for the smaller notch seen in the measurements.

Through additional measurements with a calibrated accelerometer (Analog devices model ADXL 320), it was determined that a force of 40 N could be achieved at all frequencies between 50 and 750 Hz. Another pertinent quantity, nonlinear distortion, was estimated from measurements at 300 Hz to be slightly more than 5% (mean absolute percent error) up to a force of 30 N.

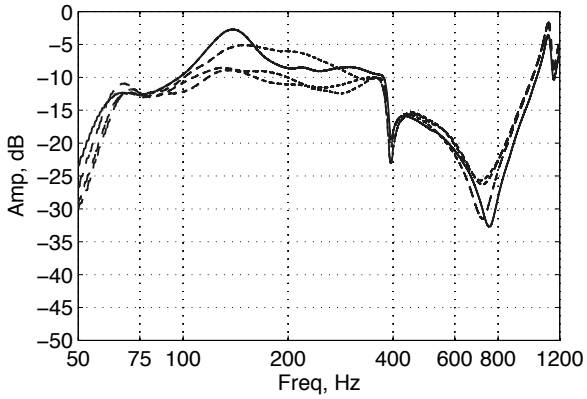

Figure 8: The measured log magnitude frequency response of the display. Measurements were taken at a point equidistant from the plate center and edge, on a line through the center, 15 degrees from the diagonal. The free response is shown with the solid line. The dashed lines show other foot-floor contact conditions with varying weight applied via the foot.

4.2 Digital correction

It is possible to improve the nominal frequency response $H_d(f)$ of the display by filtering the actuator signal $F(t)$ via a suitably designed linear, time-invariant corrective filter, H_c. Here, we concentrate on the magnitude only: H_c is designed so that the corrected device frequency response $H_{d'}(f) = H_d(f)H_c(f) \approx g$ in the band of interest, where g is a constant gain factor.

Since such a filter lacks any spatial dependency, correction is most effective below the first resonant frequency of the device, f_1, because above it the device transfer function varies across the surface of the plate (Fig. 7). As a result, correction is most useful for compensating factors, such as actuator characteristics, that can be treated as lumped parameter systems.

A compensating filter H_c was designed to equalize the device response in the frequency range from f =50 Hz to 750 Hz. It was implemented digitally as an IIR filter of order N, which was estimated using the least p-th norm optimization method [11]. Figure 9 shows a comparison of the original (free) frequency response of the device with responses corrected by filters of order $N = 10$ and 14. In the latter case, the response is flat in a passband with -10 dB roll off near 50 Hz and 750 Hz.

5 Application: Ground texture synthesis

A motivating application for the developments described above is the display of high frequency force information simulating the feel of stepping onto natural ground materials [13]. When a shoe steps onto materials like earth, grass or snow, it is subjected to interaction forces that can include: viscoelastic components, describing the recoverable deformation of the volume of the ground surrounding the contact interface; transient shock components, from the impact of toe and heel against the ground; and plastic components from the collapse of air pockets, brittle structures or granular force chains, resulting in unrecoverable deformation [2, 8]. Combinations of such effects give rise to low-frequency forces and high frequency, texture-like vibrations that are characteristic of human walking on different surfaces [7]. A simple example of a point-interaction model for such behaviors is the lumped parameter stick-slip unit shown in Fig. 10. In the stuck state, it behaves like a viscoelastic element with the parameters indicated. When the force on the plastic unit exceeds a (stochastic) threshold value, a slip event is generated, and is rendered using an event-based approach [13]. High frequency components of these transient events depend in detail on the materials and forces of interaction [14]. A high fidelity vibrotactile display such as that presented here is useful for reproducing such events without artifacts.

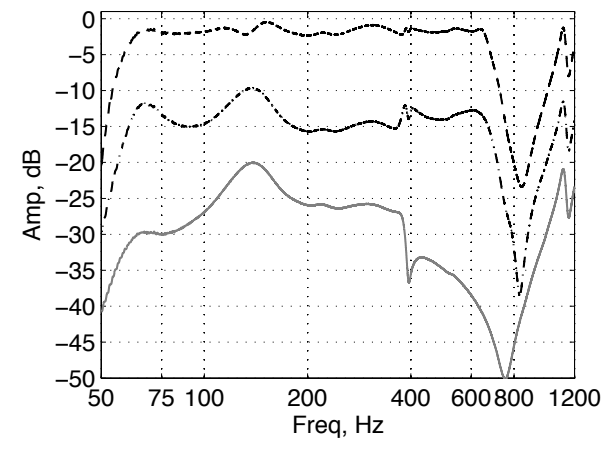

Figure 9: Bottom: Measured device frequency response without foot contact. Middle: Same response after correction by an IIR filter of order $N = 10$. Top: Response corrected with filter of order $N = 14$. The plotted amplitudes are offset for clarity of presentation. The y-axis labels (in dB) are intended to indicate variation rather than absolute amplitude.

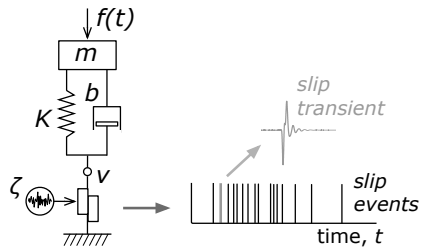

Figure 10: An abstracted point interaction model for natural ground materials. It is characterized by lumped parameters describing the mass m, stiffness K, and damping b together with the stochastic threshold ζ. In one embodiment, slip events are rendered using a physically based model of impact transients (not shown here) [14].

6 Conclusion

We have presented a vibrotactile display device integrated in a rigid surface, consisting of an actuated and instrumented floor tile. The analysis considered factors affecting the bandwidth of the device, including the response of the elastic suspension and rigid plate, the actuator coupling, and the static deflection of the suspension under load by a human foot. The plate was implemented as a lightweight

composite sandwich panel constructed from aluminum honeycomb. A digital filter was designed to compensate for artifacts in the measured frequency response. The device allows for accurate reproduction of frequencies between about 50 and 750 Hz.

The device is simple, and designed to be easily reproducible or adaptable to the demands of various applications or research tasks [14, 15]. Formulae such as Eq. (4) indicate how the response characteristics of the display can be expected to scale with system dimensions.

Despite these results, a number of areas can be identified in which the device might be improved. They include:

- *Plate material selection:* As presented in the analysis, a composite panel similar to that used in the prototype, but constructed from a honeycomb core with larger thickness h, and greater facing thickness t_f would achieve a usable bandwidth that extends to higher frequencies. The first resonant frequency of the plate scales as $\sqrt{t_f h}$ in the thin plate approximation (which will require corrections if the plate or facings are too thick).

- *Actuator design:* The large voice coil actuator used in the present device introduces significant coloration in the frequency response of the device, much of which can be equalized. A better response may be achieved through the use of smaller, more efficient voice coil motors coupled to the structure in a spatial configuration chosen to optimize the device transfer function.

- *Vibration control:* Active structural vibration control strategies exist that could improve the fidelity of such a display using arrays of surface mounted sensors and actuators, together with closed-loop controllers [1, 9, 10]. Such techniques might be used to achieve accurately controlled vibrational responses under a wider array of contact loads.

In ongoing research in our lab, the device is being utilized to study the rendering and display of virtual ground surface properties, related aspects of haptic perception, and the integration of such display components in multimodal virtual and augmented reality environments [16].

Acknowledgements

The authors gratefully acknowledge support from the MDEIE of Quebec for the EU FP7 project NIW (no. 222107). The first author acknowledges support from the ESF COST Action on Sonic Interaction Design (no. IC0601).

References

[1] K. Chandrashekhara and A. Agarwal. Active vibration control of laminated composite plates using piezoelectric devices: a finite element approach. *Journal of Intelligent Material Systems and Structures*, 4(4):496, 1993.

[2] S. Dixon and A. Cooke. Shoe-Surface Interaction in Tennis. *Biomedical engineering principles in sports*, page 125, 2004.

[3] N. Fletcher and T. Rossing. *The physics of musical instruments*. Springer Verlag, 1998.

[4] J. Kee Paik, A. Thayamballi, and G. Sung Kim. The strength characteristics of aluminum honeycomb sandwich panels. *Thin-walled structures*, 35(3):205–231, 1999.

[5] P. M. Kennedy and J. T. Inglis. Distribution and behaviour of glabrous cutaneous receptors in the human foot sole. *The Journal of Physiology*, 583(3), 2002.

[6] L. Meirovitch. *Dynamics and control of structures*. John Wiley & Sons, 1990.

[7] J. Sabatier and A. Ekimov. A Review of Human Signatures in Urban Environments Using Seismic and Acoustic Methods. In *2008 IEEE Conference on Technologies for Homeland Security*, pages 215–220, 2008.

[8] V. Stiles, I. James, S. Dixon, and I. Guisasola. Natural Turf Surfaces: The Case for Continued Research. *Sports Medicine*, 39(1):65, 2009.

[9] U. Stobener and L. Gaul. Modal vibration control for PVDF coated plates. *Journal of Intelligent Material Systems and Structures*, 11(4):283, 2000.

[10] N. Tanaka and T. Sanada. Modal control of a rectangular plate using smart sensors and smart actuators. *Smart Materials and Structures*, 16(1):36–46, 2007.

[11] J. Taylor and Q. Huang. *CRC handbook of electrical filters*. CRC, 1997.

[12] M. Trulsson. Microreceptive afferents in the human sural nerve. *Exp Brain Res*, 137:111–116, 2001.

[13] Y. Visell, J. Cooperstock, B. Giordano, K. Franinovic, A. Law, S. McAdams, K. Jathal, and F. Fontana. A Vibrotactile Device for Display of Virtual Ground Materials in Walking. *Lecture Notes in Computer Science*, 5024:420, 2008.

[14] Y. Visell, F. Fontana, B. Giordano, R. Nordahl, S. Serafin, and R. Bresin. Sound design and perception in walking interactions. *International Journal of Human-Computer Studies*, 2009.

[15] Y. Visell, A. Law, and J. Cooperstock. Touch Is Everywhere: Floor Surfaces as Ambient Haptic Interfaces. *IEEE Transactions on Haptics*, 2009.

[16] Y. Visell, A. Law, J. Ip, R. Rajalingham, S. Smith, and J. R. Cooperstock. Interaction Capture in Immersive Virtual Environments via an Intelligent Floor Surface. In *IEEE Virtual Reality*, 2010 (Submitted).